

THE OHIO STATE UNIVERSITY

CENTER FOR EMERGENT MATERIALS

SUMMER REU RESEARCH REPORT



---

# 2D Material Modeling with Density Functional Theory: Applications in Scanning Tunneling Microscopy

---

*Author:*  
Stephen GANT

*Advisor:*  
Dr. Jay GUPTA  
*Mentor:*  
Jacob REPICKY

July 28, 2018

# Contents

<b>Abstract</b>	<b>2</b>
<b>1 Introduction</b>	<b>2</b>
1.1 Motivations . . . . .	2
1.2 The Many-Body Problem . . . . .	2
1.2.1 Formulation . . . . .	2
1.2.2 Difficulties . . . . .	2
1.2.3 Approaches . . . . .	3
1.3 Crystal Structure . . . . .	3
1.3.1 Lattices . . . . .	3
1.3.2 Surfaces . . . . .	4
1.3.3 Reciprocal Space . . . . .	5
<b>2 Methods</b>	<b>7</b>
2.1 STM . . . . .	7
2.1.1 Introduction . . . . .	7
2.1.2 Scanning Modes . . . . .	7
2.2 DFT . . . . .	8
2.2.1 Basic Theory . . . . .	8
2.2.2 Implementation . . . . .	8
2.2.3 Calculation Details . . . . .	9
<b>3 Results</b>	<b>9</b>
3.1 Surface Relaxation . . . . .	9
3.2 Band Structure . . . . .	10
3.2.1 Ir(111) . . . . .	10
3.2.2 Fe/Ir(111) . . . . .	10
3.3 LDOS . . . . .	11
3.3.1 Ir(111) . . . . .	11
3.3.2 Fe/Ir(111) . . . . .	11
3.4 STM Images . . . . .	11
<b>4 Conclusion</b>	<b>12</b>
<b>5 Future Research</b>	<b>12</b>
<b>References</b>	<b>12</b>

# Abstract

This project aims to develop DFT modeling techniques for use in STM analysis. By simulating Ir(111) and Fe/Ir(111)—for which experimental data already exist in-lab—an analysis of the effectiveness of current techniques in DFT is performed. The techniques are capable of modeling the basic behavior of Ir(111). They accurately reproduce surface relaxation spacing and topography, while producing a somewhat accurate LDOS. Band structure calculations also appear normal. Fe/Ir(111) calculations also appear promising in the aforementioned areas, with the exception of the LDOS for which no viable experimental data exist for comparison. Overall, this project has aided the development of proficient DFT modeling in the group’s arsenal of analytic tools.

## 1 Introduction

### 1.1 Motivations

It has long been known that surfaces of materials ought to display unique properties different than those of the bulk.<sup>1</sup> This fact has led to continued interest in the development and utility of nanomaterials whose properties are dominated by surface effects. More recently, the discovery and characterization of graphene has greatly heightened interest in the field.<sup>2</sup> These nanomaterials can exhibit exceptional properties.<sup>3,4,5</sup> Some are so special that they have been given their own names: topological insulators<sup>6,7,8</sup> and skyrmion lattices<sup>9</sup> to name a few.

Experimentally identifying and probing these surfaces is of great importance for future research but can only extensively be done by a handful of techniques such as angle-resolved photo emission spectroscopy (ARPES) or scanning tunneling microscopy (STM).<sup>10</sup> In the case of STM, it can often be difficult to interpret observed data due to the wide variety of contributing factors at play. Thus, having accurate theoretical models of specific systems under study can be quite advantageous for establishing confident analysis.<sup>11</sup> This project aims to implement density functional theory (DFT), one such theoretical method, for the purpose of modeling STM data.

### 1.2 The Many-Body Problem

#### 1.2.1 Formulation

In order to accurately model atomically periodic systems, the many-body Schrödinger equation must be solved.

$$\begin{aligned} i\hbar \frac{\partial}{\partial t} \Psi &= \hat{H} \Psi, \\ \hat{H} &= -\frac{\hbar^2}{2m_e} \sum_i \nabla_i^2 - \sum_{i,I} \frac{Z_I e^2}{|\mathbf{r}_i - \mathbf{R}_I|} \\ &+ \frac{1}{2} \sum_{i \neq j} \frac{e^2}{|\mathbf{r}_i - \mathbf{r}_j|} - \sum_i \frac{\hbar^2}{2M_I} \nabla_I^2 \\ &+ \frac{1}{2} \sum_{I \neq J} \frac{Z_I Z_J e^2}{|\mathbf{R}_I - \mathbf{R}_J|} \end{aligned} \quad (1)$$

Electrons and nuclei are denoted by lower and upper case indicies and radii respectively.<sup>10,12</sup>

#### 1.2.2 Difficulties

Many-body problems in physics are notoriously challenging. Even the classical three-body problem has no general closed form solution,<sup>13</sup> let alone the quantum N-body problem. In fact, naively looking for solutions to eq. 1.2.1 involves finding eigenvectors in a space that scales exponentially with N.<sup>12</sup> This makes such a problem effectively impossible for large N systems even given modern computing power.

### 1.2.3 Approaches

Many clever approximations must be made to arrive at solutions that are a reasonable compromise between accuracy and computing cost. (Note: while some of the approximations discussed below are unique to DFT, many apply to N-body problems at large). These approximations include:

- **The Born Oppenheimer Approximation:** Due to the fact that  $M_I \gg m_e$  in (1.2.1), the atomic nuclei can be assumed to be stationary. This makes the final two terms in eq. 1.2.1 constant (the 4<sup>th</sup> being zero and the 5<sup>th</sup> being non-zero) and removable via a shift in the total energy of the system. Thus, the Hamiltonian can be reformatted as<sup>12</sup>

$$\hat{H} = \hat{T}_{kin} + \hat{V}_{nuc} + \hat{V}_{ee} \quad (2)$$

- **Quantization of Continuous Variables and Termination of Infinite Sets:** Under a good set of basis functions, integrals and sums involved in solving the N-body problem ought to converge to the correct answer within a reasonable number of terms. This allows for finer integration meshes and higher index terms to be neglected safely.
- **Periodic Boundary Conditions:** Since the systems of interest to STM are almost always crystalline and fairly large ( $N \approx 10^{23}$ ), it becomes convenient to assume that the material is constructed via infinitely repeating *unit cells*. This behavior is modeled by assuming that once the end of a unit cell is reached it *loops back*. Mathematically, this means that

$$\Psi(\mathbf{r} + \mathbf{a}_i) = \Psi(\mathbf{r}) \quad (3)$$

where  $\mathbf{r}$  is a vector in the unit cell and  $\mathbf{a}_i$  is one of the vectors defining the size of the unit cell. Further discussion can be found in 1.3.1.

- $\Psi \rightarrow n$ : Instead of searching for the eigenfunctions of various energy levels, it's easier to look for the electron density of the ground state ( $n$ ), which turns out to be a viable quantity for computing nearly all other relevant parameters of a system.<sup>10</sup> In fact, this is where DFT gets its name from as the system's parameters become functionals of the electron density.<sup>14</sup>

## 1.3 Crystal Structure

### 1.3.1 Lattices

Fundamentally, the structure of a material (and its atomic species) determines what its properties are. Thus, it is essential that it is modeled correctly. Luckily, one of the hallmarks of materials—esp. those under study by STM—is their periodicity. As such, it is possible to represent their structure using what is called a unit cell. A unit cell is defined as a minimal building block such that tessellating it reproduces the complete structure of the material.

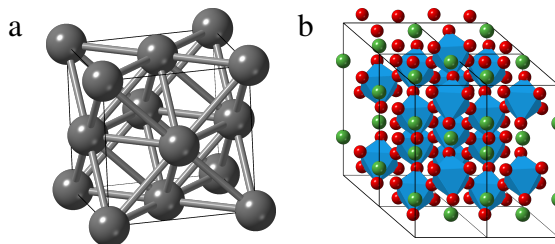


Figure 1: **(a)** A depiction of Ir, which has a face-centered cubic (FCC) unit cell. **(b)** A depiction of LaAlO<sub>3</sub>, which can be represented by a trigonal unit cell.

Mathematically, an  $n$ -dimensional lattice can be represented by  $n$  lattice vectors  $\{\mathbf{a}_1, \dots, \mathbf{a}_n\}$  and what is known as a *basis*. The lattice vectors define the boundaries of the unit cell such that translation by any linear combination of them with integer coefficients brings one back to the same relative point in the unit cell. The basis is a set of vectors  $\{\mathbf{v}_1, \dots, \mathbf{v}_n\}$

that defines the positions of the atoms within the unit cell.

A common family of crystals are cubic lattices. The most densely packed member of this family is the face-centered cubic (FCC) lattice (Figure 1a), which is constructed by placing atoms on the center of each face and corner of the cube. In terms of lattice vectors and a basis, the FCC lattice can be represented by

$$\begin{aligned} \mathbf{a}_1 &= a\hat{x}, & \mathbf{a}_2 &= a\hat{y}, & \mathbf{a}_3 &= a\hat{z} \\ \mathbf{v}_1 &= 0, & \mathbf{v}_2 &= \frac{1}{2}\mathbf{a}_1 + \frac{1}{2}\mathbf{a}_2, \\ \mathbf{v}_3 &= \frac{1}{2}\mathbf{a}_1 + \frac{1}{2}\mathbf{a}_3, & \mathbf{v}_4 &= \frac{1}{2}\mathbf{a}_2 + \frac{1}{2}\mathbf{a}_3 \end{aligned} \quad (4)$$

where  $a$  is a lattice constant dependent on the material. Many transition metals like Ir have this structure. Beyond cubic lattices, there are more non-trivial constructions like the trigonal unit cell depicted in Figure 1b.<sup>15,16</sup>

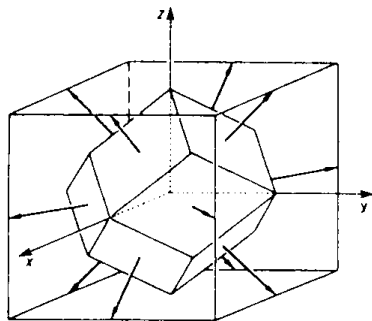


Figure 2: A depiction of a FCC Wigner-Seitz cell.<sup>17</sup>

It is worth noting that a particular unit cell representation is not necessarily unique. Oftentimes it is possible to represent a crystal using an entirely different scheme. For instance, FCC lattices can be represented using a trigonal scheme as well.<sup>10</sup> More fundamentally, it is possible to construct a unit cell that occupies a minimal possible volume known as a *primitive cell*. One popular type of primitive cell is the Wigner-Seitz cell, which is constructed by the area contained within orthogonal planes that bisect the vectors between nearest neighbor atoms (Figure 2).

Of particular relevance to experimental setups is the orientation of a crystal. For instance, in B20 crystal structures it's relevant whether or not the crystal is upside down or not.<sup>18</sup> As such, it is conventional to denote a crystal's orientation using what are known as Miller indices. These indices define a vector (composed of the lattice constants in each direction) which in turn defines a plane that is perpendicular to the vector (see Figure 3). The analysis of this report focuses on Ir cut along the [111] plane (Ir(111)) corresponding to the crystal for which experimental STM data have been taken.

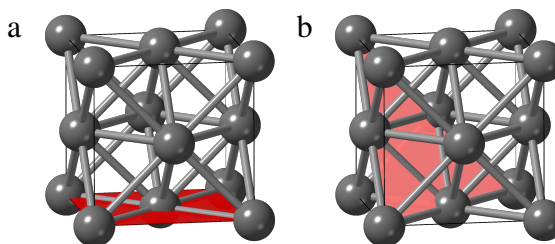


Figure 3: (a) A [010] Miller plane superimposed on a FCC unit cell. (b) A [111] Miller plane superimposed on a FCC unit cell.

### 1.3.2 Surfaces

A uniquely important component of modeling nanomaterials is accurately representing surfaces and how films interface with the substrate they are grown on. This requires constructing a unit cell that is much larger/taller than usual, a supercell, with a significant portion being empty (Figure 4a). Since periodic boundary conditions are still in effect, this supercell construction is registered in the computer as a system of infinite slabs of material separated by enough vacuum to decouple inter-slab interactions. A further wrinkle to the supercell construction is that the orientation and cut of the crystal become relevant variables that must be accounted for. In the case of a FCC(111) crystal, a trigonal supercell was used to accurately model the [111] surface while allowing for adequate vacuum space by adjusting the height. An isolated slab of Ir(111) using

this supercell can be seen in Figure 4c. Another key structural property of surfaces is that their inter-atomic spacing almost always changes due to the lack of atoms above the surface. This process is known as *relaxation* and can be fairly nontrivial.<sup>10,19</sup>

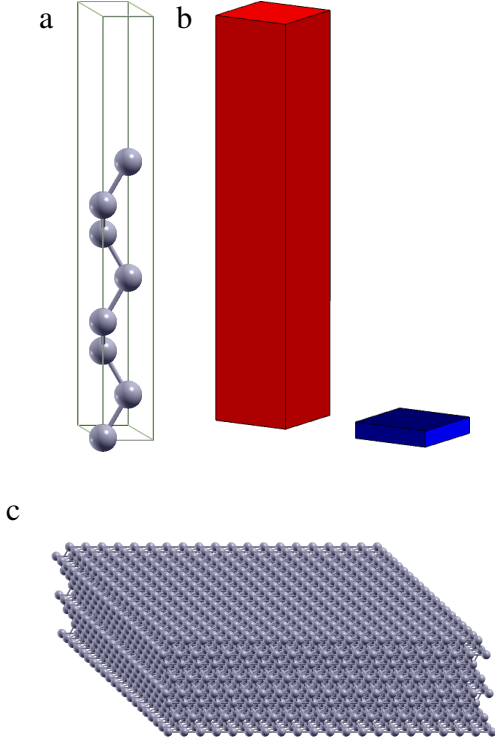


Figure 4: **(a)** An Ir(111) supercell.<sup>20</sup> **(b)** A depiction of how a real-space supercell (red) changes in reciprocal space (blue). **(c)** Ir(111) slab.<sup>20</sup>

### 1.3.3 Reciprocal Space

In order to understand the electronic structure of a material, it is often convenient to consider how electrons are distributed in energy-momentum space. It is conventional, however, to consider the electrons' wavevector  $k$  as a proxy of its momentum. Keeping in mind that  $k$  has units of  $\frac{1}{\text{space}}$  it becomes possible to represent electrons' momentum in *reciprocal space*.

In fact, the entire lattice structure can be inverted into reciprocal space with its own set of

reciprocal lattice vectors  $\{\mathbf{b}_1, \dots, \mathbf{b}_n\}$ . In three dimensions, these vectors are

$$\begin{aligned} \mathbf{b}_1 &= \frac{2\pi}{V}(\mathbf{a}_2 \times \mathbf{a}_3), & \mathbf{b}_2 &= \frac{2\pi}{V}(\mathbf{a}_3 \times \mathbf{a}_1), \\ \mathbf{b}_3 &= \frac{2\pi}{V}(\mathbf{a}_1 \times \mathbf{a}_2) \end{aligned} \quad (5)$$

where  $V$  is the volume of the unit cell in real space.

Within reciprocal space, it is customary to represent the possible  $k$  values within a Wigner-Seitz cell with the center being the origin (Figure 5a). This cell is often referred to as the 1<sup>st</sup> Brillouin zone (BZ). Depictions of the 1<sup>st</sup> BZ for FCC and trigonal lattices can be seen in Figures 5b,d. Also labeled are high symmetry points which define what is known as the *irreducible Brillouin zone* (IBZ). The IBZ is the smallest possible cut of  $k$  space that can still represent the whole BZ via physical and lattice symmetries (time reversal, mirror, etc.).<sup>21,22,23</sup>

When dealing with surfaces it is also necessary to observe the  $k$ -space of a supercell. In this case, the height of the 1<sup>st</sup> BZ becomes very compressed (Figure 4b). For a simple trigonal or tetragonal supercell of height  $h_{\text{real}} = \alpha a$ , its reciprocal height becomes  $h_{\text{recip}} = \frac{2\pi}{\alpha a}$ , giving a scaling that goes like

$$\frac{h_{\text{real}}}{h_{\text{recip}}} \propto \alpha^2 \quad (6)$$

Since  $\alpha \sim 10$  for most relevant calculations,  $\frac{h_{\text{real}}}{h_{\text{recip}}} \sim 100$ . Thus the surface supercell BZ can be thought of as a flat projection of the bulk BZ (Figure 5c).

Due to the fact that electrons are fermions, they cannot occupy the same quantum state and end up spread out in  $k$ -space. The surface of the shape representing the electrons' momenta is known as the Fermi surface (Figure 6). Depending on the number of electrons, it can extend into the 2<sup>nd</sup>, 3<sup>rd</sup>, etc. BZ. The electrons on this surface represent the most energetic occupied states in the material. The energy that these electrons have is called the Fermi energy and it plays a

crucial role in determining the basic fundamental properties of a material.

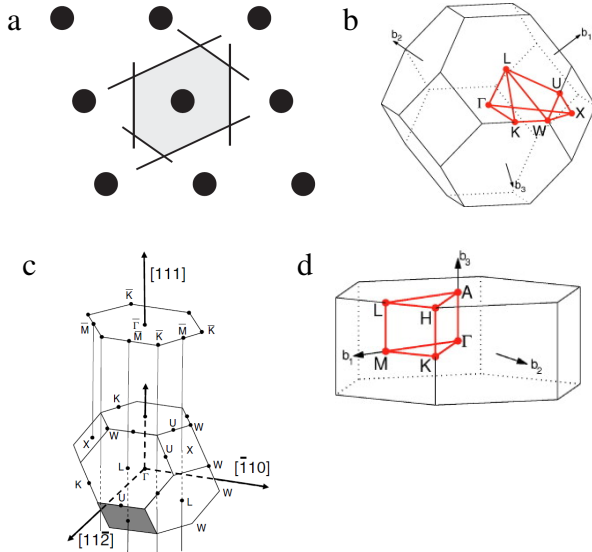


Figure 5: **(a)** A depiction of how the 1<sup>st</sup> Brillouin zone (BZ) is constructed.<sup>24</sup> **(b)** The 1<sup>st</sup> BZ of a FCC lattice.<sup>25</sup> **(c)** A depiction of the projected [111] surface 1<sup>st</sup> BZ of a FCC lattice.<sup>26</sup> **(d)** The 1<sup>st</sup> BZ of a Trigon lattice.<sup>25</sup>

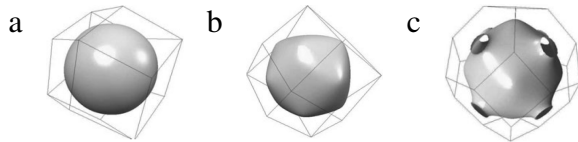


Figure 6: Fermi surfaces of: **(a)** Potassium. **(b)** Lithium. **(c)** Copper.<sup>16</sup>

For any given momentum there are numerous continuous *bands* it can occupy (Figure 7). If bands go through the Fermi energy, the material is a metal. If not, it is either a semiconductor or an insulator depending on how wide of a gap exists between the lowest-energy unoccupied band and the highest-energy valance band. Accurately representing these bands becomes increasingly challenging as a system's dimensionality increases since they exist in  $n + 1$  dimensions ( $n$  for  $k$  and one for  $E$ ). In three dimensions, it is customary to represent the bands as the  $E$ - $k$  plots produced by following a set of linear paths in  $k$ -space between high symmetry points.

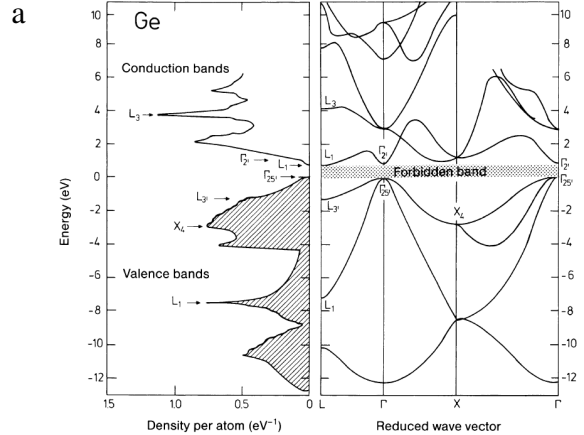


Figure 7: Semiconductor (Ge) band structure and corresponding DOS.<sup>27</sup>

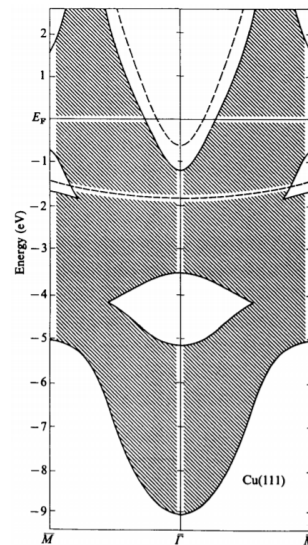


Figure 8: An example of the surface states in Cu(111), depicted as the lone bands outside the shaded bulk projected band structure.<sup>28</sup>

When comparing bulk band structures to those of a surface, it is customary to project the bulk band structure onto the virtually flat supercell BZ. This is done by taking a high symmetry path that is perpendicular to the surface vector and plotting the band structures for all possible values of  $k_{\perp}$ . This is known as the *bulk projected band structure* (BPBS). Computationally this is done by looking at a set of  $k_{\perp}$  values  $\{0, \dots, k_{\perp,max}\}$  with relatively small spacing. Plots of the BPBS and surface bands can be used to identify surface states. Surface bands that lie

outside the bulk bands are such states (Figure 8).<sup>10,26</sup>

## 2 Methods

### 2.1 STM

#### 2.1.1 Introduction

Scanning tunneling microscopy was first developed by Binnig and Rohrer in 1982 as a method to probe the surface structure of materials.<sup>29</sup> At a basic level, it uses tunneling currents through a biased vacuum to probe the electronic structure of a material (see Figure 9).

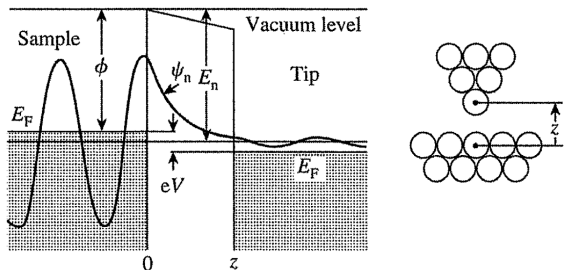


Figure 9: A pictorial representation of tip-sample electron tunneling<sup>29</sup>

In order to achieve this feat, STM is typically performed in ultra-high vacuum (UHV) environments often at very low temperatures ( $\sim 5$  K). Using piezoelectric stacks on a vibration insulated stage, a metal tip is brought mere angstroms away from the surface under investigation to establish a tunneling current. This current is roughly exponentially dependent on  $\Delta z$  making it quite useful for probing very small height changes like those of atoms on the surface of a material.

#### 2.1.2 Scanning Modes

While STM has a number of versatile applications this report focuses on the two most commonly used: constant current mode and spectroscopy mode

- **Constant Current:** Under this mode, a preselected current is locked onto and maintained via a feedback loop with the  $z$ -direction piezos. The tip is then systematically moved over the surface while the relative changes in  $z$  are recorded. This results in a topographic map of the electronic states of the system according to the equation

$$\Delta z(x, y) = -\frac{\Delta I(x, y)}{dI(z)/dz}. \quad (7)$$

It is worth noting that this image can vary significantly depending on the voltage the sample is biased at as some atomic species may only appear at certain biases<sup>29,30</sup> (Figure 10).

- **Spectroscopy:** Scanning tunneling spectroscopy (STS) mode measures  $\frac{dI}{dV}(V)$  at a localized point on the surface. These data happen to be directly correlated to energy-projected band structure at a given point—also known as the local density of states (LDOS).

$$\frac{dI}{dV}(V) \propto n_{surface}(E_{Fermi} + eV) \quad (8)$$

Thus, the band structure of a material can be locally probed, offering significant insight into the electronic structure of the surface.

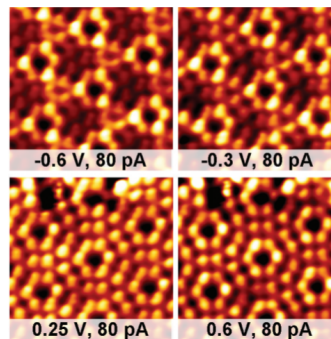


Figure 10: The famous (7x7) reconstruction of Si(111). The dependence on bias can clearly be seen.<sup>31</sup>

## 2.2 DFT

### 2.2.1 Basic Theory

As discussed previously, DFT is a way of modeling materials via approximating the ground state electron density. In 1965, Kohn and Sham devised a scheme (the modern equivalent of which is seen in Figure 11) wherein non-interacting electron wavefunctions (corresponding to  $V_{Har}$ ) coupled with a reasonable scheme for modeling the electron exchange correlation energy (corresponding to  $V_{xc}$ ) could be used to iteratively converge on a ground-state electron density  $n(\mathbf{r})$ .

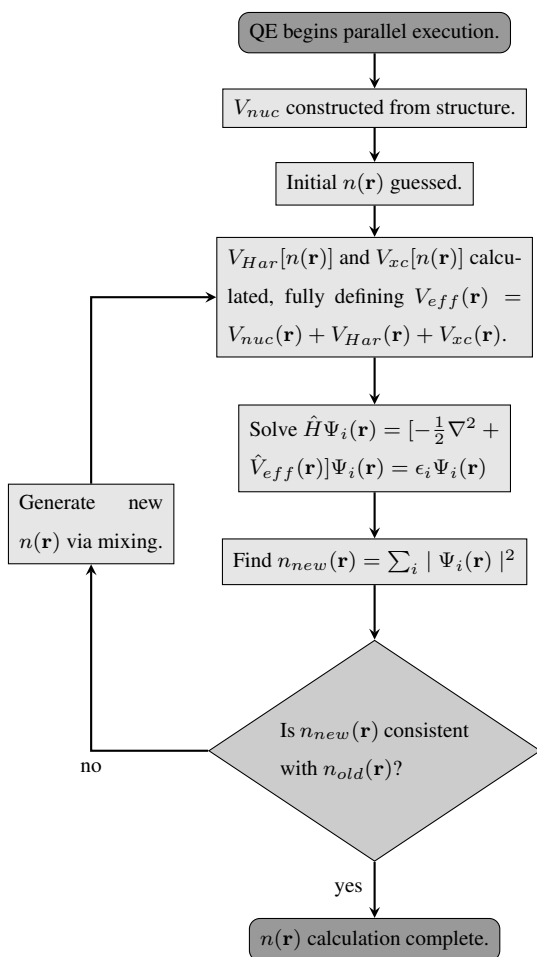


Figure 11: A depiction of how the Kohn-Sham equations are solved.<sup>10</sup>

### 2.2.2 Implementation

It took many more decades for DFT algorithms to become as versatile as they are now. Some of the characteristic parameters in DFT for one to be aware of are:

- **Pseudopotentials:** Modeling all electrons in a system is quite computationally taxing. Instead, DFT calculations use pseudopotentials, which are modified atomic potentials that only include valence electrons under the influence of a charge-screened core. Additionally, the core portion of wavefunctions is often modified to be smoother such that it takes fewer higher energy terms in a given basis to model (Figure 12).<sup>32</sup>

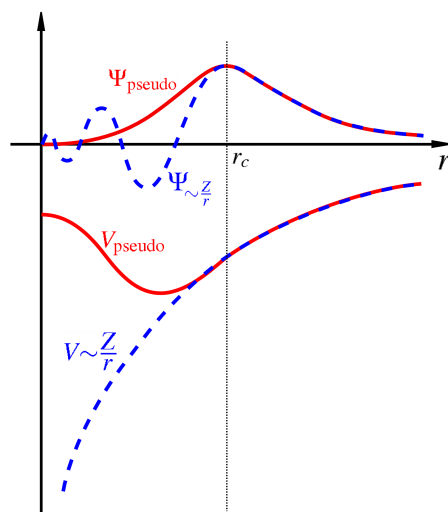


Figure 12: A comparison between pseudopotentials (red) and real potentials (blue).

- **Energy Cutoff:** Wavefunctions are approximated using some basis. In order to save computing power, only the first few dozen basis functions under a specified energy cutoff are used. This almost always works well since higher order terms are outside the energy scope of the problem. This approximation is further aided by the use of pseudopotentials.

tials which smooth out higher frequency modes of  $\Psi$  near the nucleus.

- **$k$ -Space Mesh:** Many computations involve integrating over  $k$ -space. Instead, it is convenient to sample  $k$ -space at a given set of points.
- **$n$  Mixing:** Oftentimes the electron density will converge more quickly if the input into the next iteration is a superposition of various previous states.
- **Smearing:** Due to sharp Fermi surface behavior in metals it is usually necessary to use some kind of smearing scheme to prevent issues in computation.

### 2.2.3 Calculation Details

Calculations were performed at the Ohio Supercomputing Center (OSC)<sup>33</sup> (see Figure 14) using the open-source DFT package Quantum Espresso (QE).<sup>34,35</sup> Pseudopotentials were taken from pslibrary1.0.0.<sup>36</sup> Using QE, both Ir(111) and Fe/Ir(111) were simulated. The Ir(111) slab was modeled using an 8 atom thick supercell, and the Fe was included by adding an additional layer onto the 8 atom thick slab (Figure 13). The number of layers was chosen as a compromise between other calculations in literature that used more atoms and the computational cost of doing so.<sup>37</sup> Ir(111) was modeled both with and without spin orbit coupling (SOC) whereas Fe/Ir(111) was modeled without any spin-ordering.

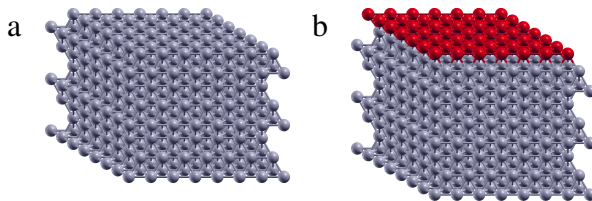


Figure 13: (a) Ir(111) slab. (b) Fe/Ir(111) slab.

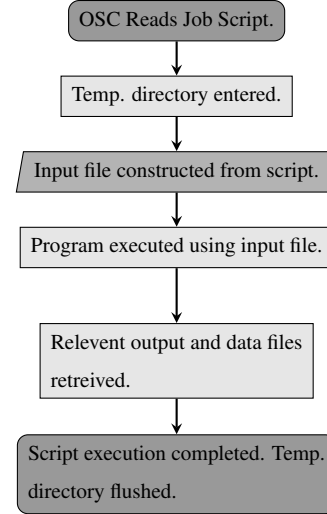


Figure 14: A depiction of the overall algorithm submitted to the supercomputer.

## 3 Results

### 3.1 Surface Relaxation

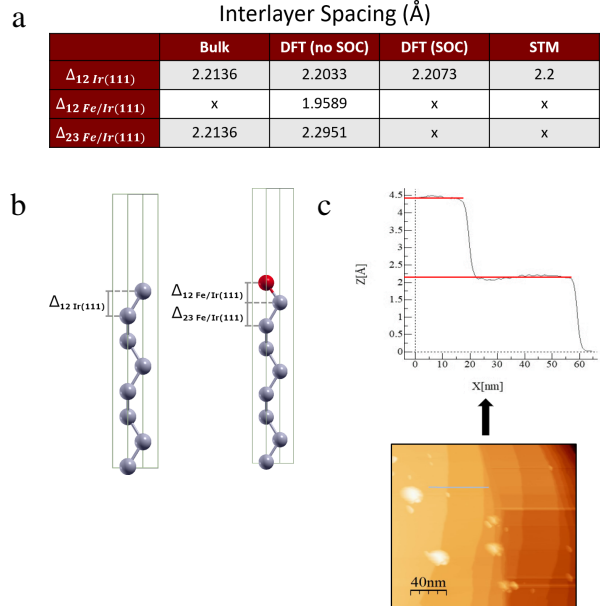


Figure 15: (a) Structural relaxation data. (b) Visual representations of the interlayer spacings. (c) Experimental data for Ir(111) (processed in WSxM<sup>38</sup>). The data seem to match what is predicted.

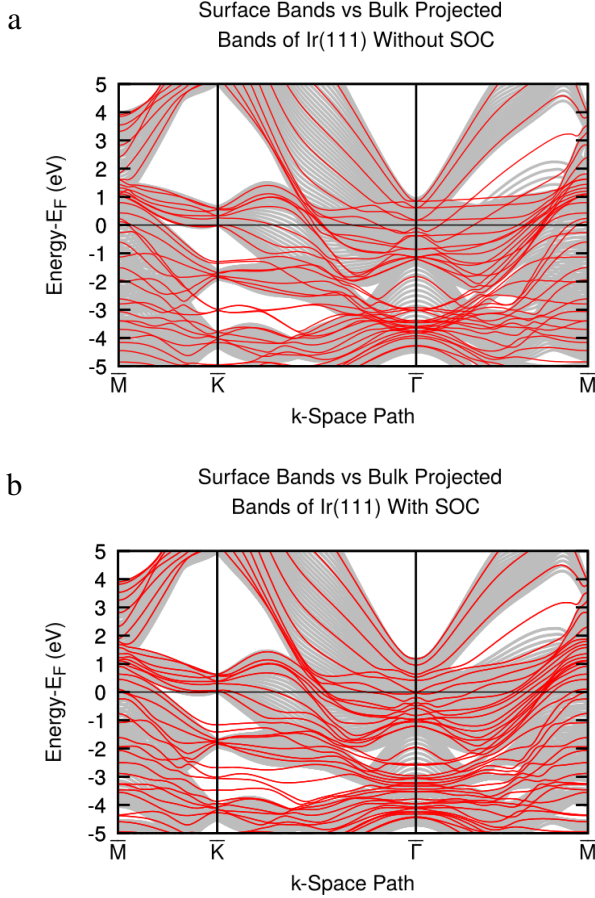


Figure 16: **(a)** Bulk projected band structure vs. slab supercell band structure of Ir(111) without SOC. **(b)** Bulk projected band structure vs. slab supercell band structure of Ir(111) with SOC.

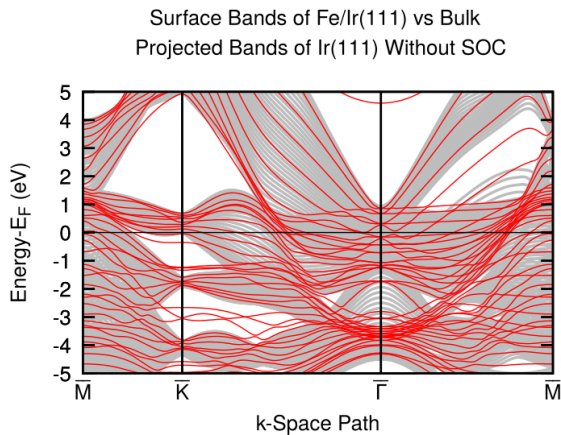


Figure 17: Bulk projected band structure of Ir(111) vs. slab supercell band structure of Fe/Ir(111).

Relaxation calculations for Ir(111) show

(Figure 15) that the inter-layer spacing grows from its value of 2.2136 Å in the bulk<sup>39</sup> to 2.2033 Å or 2.2073 Å—depending on whether or not SOC is accounted for—at the surface. These results correspond well with experimental measurements as well as predictions from literature.<sup>37</sup> Calculations for Fe/Ir(111) indicate the Fe layer is closer to the Ir substrate than the spacing between Ir layers (1.9589 Å) and that the Fe layer seems to pull on the top Ir layer enough to increase its spacing by  $\sim 0.1$  Å. These results correspond well with the literature<sup>40</sup> and make further sense when the inter-atomic spacing for Fe is noted to be less than that of Ir.<sup>41</sup>

## 3.2 Band Structure

### 3.2.1 Ir(111)

Supercell band structure calculations follow the  $M - K - \Gamma - M$  path depicted in Figure 4d and are drawn in red. Bulk projected band structures follow the  $\bar{M} - \bar{K} - \bar{\Gamma} - \bar{M}$  path depicted in Figure 4c and are drawn in gray. In order to represent bulk behavior, 20 linearly spaced values of  $k_{\perp}$  from 0 to  $k_{\perp,max}$  were used (see Figure 16).

Multiple surface states were observed at  $K$  in both plots, with another clear surface state seen between  $\Gamma$  and  $M$ . The introduction of SOC appears to spread the bands apart slightly as can be seen at  $\Gamma$  as expected. Moreover, multiple bands cross at the Fermi level, suggesting metallic behavior as expected for Ir which is a transition metal.

### 3.2.2 Fe/Ir(111)

The Fe/Ir(111) bands follow the same path as those of Ir(111) with the same number of  $k_{\perp}$  values taken into account for bulk bands (see Figure 17).

Surface states are also observed, and while most are quite similar in nature to those of bare Ir(111), there is a new surface state observed

at  $K$  just below the Fermi level. Additionally, metallic behavior is observed as expected.

### 3.3 LDOS

#### 3.3.1 Ir(111)

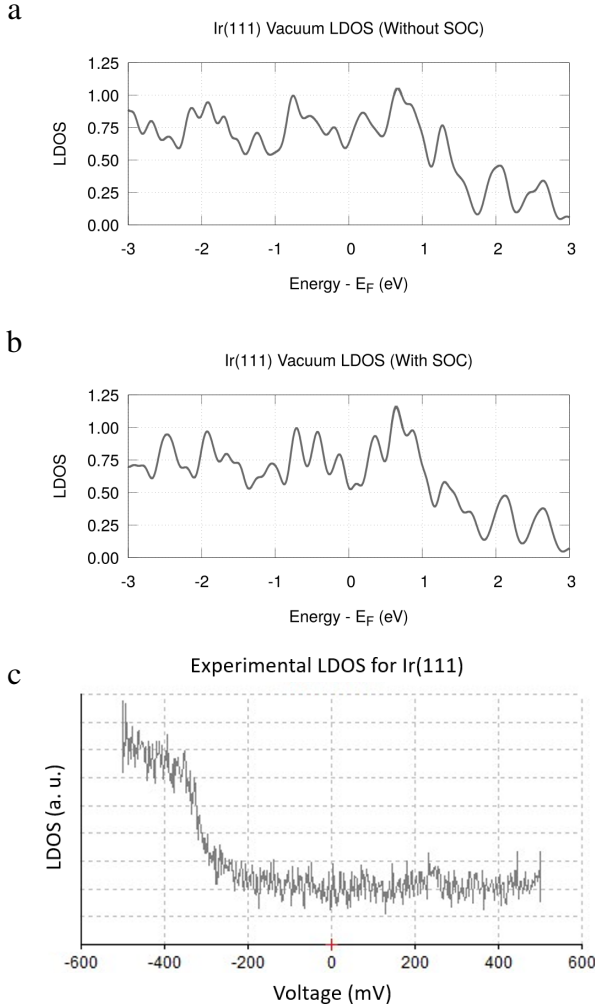


Figure 18: (a) Simulated LDOS of Ir(111) without SOC. (b) Simulated LDOS of Ir(111) with SOC. (c) Experimentally observed LDOS of Ir(111).

As can be seen in Figure 18, the LDOS seem to match qualitatively, reproducing the ridge behavior observed in experiment. This ridge behavior observed at around  $\sim 1.2$  eV in theory is due to the bunching of local extrema in the band structures. There appears to be a  $\sim 1.5$

eV mismatch between where this ridge behavior occurs in experiment. This is likely due to a variety of factors including intrinsic uncertainty in the Fermi level in DFT calculations, STM's tendency preferentially sample near  $\Gamma$ , and the dependence of experimental LDOS data on the STM's tip. SOC appears to have a minimal effect. However, the spreading out of bands can be observed as a small dip in the simulated LDOS near  $E = 0$  eV.

#### 3.3.2 Fe/Ir(111)

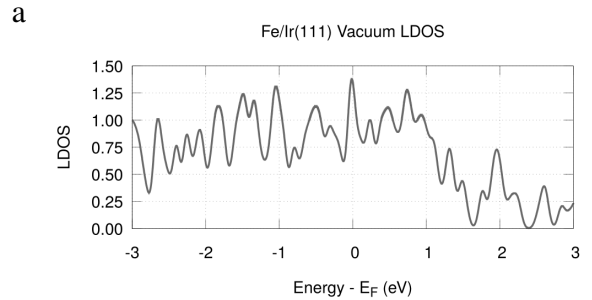


Figure 19: Simulated LDOS of Fe/Ir(111).

Similar ridge behavior is observed for Fe/Ir(111) (Figure 19). Additionally, there is slight slouching that occurs at lower biases that is different from Ir(111). While no viable experimental data were collected to compare the simulated data to, the qualitative observations produced in Figure 19 could be used to differentiate Fe layers from Ir layers. This task can be quite difficult due to the pseudomorphic growth of the Fe ML onto Ir(111).

### 3.4 STM Images

As can be seen in Figure 20a, the topography for Ir(111) seems to match quite well. In the case of Fe/Ir(111) (Figure 20), the topography matches more poorly. This could be due to the fact that the image was taken from the literature<sup>11</sup> and may be distorted. It's also possibly indicative of strain in the Fe ML. This could be expected since Fe prefers a smaller lattice that

than of the Ir that it is pseudomorphically grown on.

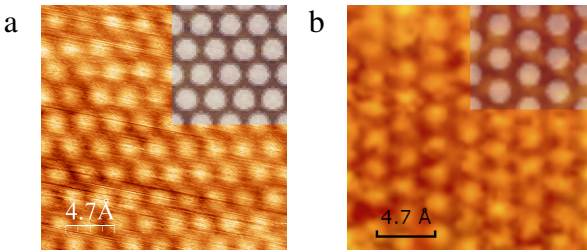


Figure 20: **(a)** STM image of Ir(111) at 0.2 V with a simulated STM image inset. **(b)** STM image of Fe/Ir(111) at 0.005 V<sup>11</sup> with a simulated STM image inset.

## 4 Conclusion

So far, the DFT simulations that have been run are able to model the basic properties of Ir(111) and Fe/Ir(111). The only exception is that the LDOS for Ir(111) appears to be off by  $\sim 1.5$  eV. Nonetheless, these preliminary results hold great promise for aiding in future experimental STM investigations.

## 5 Future Research

Further investigation is warranted in the following areas:

- **Finishing the basic analysis of Ir(111) and Fe/Ir(111):** This involves investigating the effects of thicker slabs with more vacuum, the strain in the Fe layer, better rectifying the LDOS discrepancy, and analyzing the surface states found in the band structure calculations.
- **Include spin ordering:** Modeling the effects of spin interactions on the band structure by including spin-orbit coupling (SOC) effects as well as ferromagnetic ordering in Fe is a good starting point. A

deeper exploration could include a consideration of more nontrivial magnetic ordering.<sup>42</sup>

- **Model new materials:** Once the methods developed here are able to be confidently implemented, they will be of great use in modeling future systems so that experimental analysis can be assisted in real-time.

## Acknowledgments

Special thanks go to Jacob Repicky for letting me bounce ideas off him, my adviser Jay Gupta for giving me the opportunity and guidance to work on this project, and Aravind Asthagiri for offering advice and insights for better DFT simulations.

Additionally, I would like to thank Dr. Valdes-Aguilar and Michelle McCoumbs for coordinating the CEM REU program that this work was a part of.

Funding for this research was provided by the Center for Emergent Materials: an NSF MRSEC under award number DMR-1420451

## References

- [1] William Shockley. On the Surface States Associated with a Periodic Potential. *Physical Review*, 56(4):317–323, August 1939.
- [2] B. M. Nichols, A. L. Mazzoni, M. L. Chin, P. B. Shah, S. Najmaei, R. A. Burke, and M. Dubey. Chapter Six - Advances in 2d Materials for Electronic Devices. In Francesca Iacopi, John J. Boeckl, and Chennupati Jagadish, editors, *Semiconductors and Semimetals*, volume 95 of *2D Materials*, pages 221–277. Elsevier, January 2016.

- [3] K. S. Novoselov, A. K. Geim, S. V. Morozov, D. Jiang, Y. Zhang, S. V. Dubonos, I. V. Grigorieva, and A. A. Firsov. Electric Field Effect in Atomically Thin Carbon Films. *Science*, 306(5696):666–669, October 2004.
- [4] Vinod K. Sangwan and Mark C. Hersam. Electronic Transport in Two-Dimensional Materials. *Annual Review of Physical Chemistry*, 69(1):299–325, April 2018.
- [5] Rubén Mas-Ballesté, Cristina Gómez-Navarro, Julio Gómez-Herrero, and Félix Zamora. 2d materials: to graphene and beyond. *Nanoscale*, 3(1):20–30, 2011.
- [6] Xiao-Liang Qi and Shou-Cheng Zhang. Topological insulators and superconductors. *Reviews of Modern Physics*, 83(4):1057–1110, October 2011.
- [7] Haijun Zhang and Shou-Cheng Zhang. Topological insulators from the perspective of first-principles calculations. *physica status solidi (RRL) – Rapid Research Letters*, 7(1-2):72–81.
- [8] Judy J. Cha, Kristie J. Koski, and Yi Cui. Topological insulator nanostructures. *physica status solidi (RRL) – Rapid Research Letters*, 7(1-2):15–25.
- [9] Felix Büttner, Ivan Lemesh, and Geoffrey S. D. Beach. Theory of isolated magnetic skyrmions: From fundamentals to room temperature applications. *Scientific Reports*, 8(1):4464, March 2018.
- [10] Dario Wolf Knebl. Shockley Surface States from First Principles. Master’s thesis, University of Graz, Austria, 2013.
- [11] Stefan Heinze, Kirsten von Bergmann, Matthias Menzel, Jens Brede, André Kubetzka, Roland Wiesendanger, Gustav Bihlmayer, and Stefan Blügel. Spontaneous atomic-scale magnetic skyrmion lattice in two dimensions. *Nature Physics*, 7(9):713–718, September 2011.
- [12] Richard M. Martin, Lucia Reining, and David M. Ceperley. *Interacting Electrons: Theory and Computational Approaches*. Cambridge University Press, June 2016.
- [13] Stephen Wolfram. *A new kind of science*. Wolfram Media, Champaign, IL, 2002.
- [14] David S. Sholl and Janice A. Steckel. *Density functional theory: a practical introduction*. Wiley, Hoboken, N.J, 2009. OCLC: ocn245025462.
- [15] R. J. D. Tilley. *Crystals and crystal structures*. John Wiley, Hoboken, NJ, 2006.
- [16] Steven H. Simon. *The Oxford solid state basics*. Oxford University Press, Oxford, 1st ed edition, 2013. OCLC: ocn853504907.
- [17] Energy Bands in Crystals (Fundamentals of Electron Theory) Part 2.
- [18] T. Jeong and W. E. Pickett. Implications of the B20 crystal structure for the magneto-electronic structure of  $\text{MnSi}$ . *Physical Review B*, 70(7):075114, August 2004.
- [19] Andrew Zangwill. *Physics at surfaces*. Cambridge University Press, Cambridge [Cambridgeshire] ; New York, 1988.
- [20] Anton Kokalj. Computer graphics and graphical user interfaces as tools in simulations of matter at the atomic scale. *Computational Materials Science*, 28(2):155–168, October 2003.
- [21] E. S. Tasci, G. de la Flor, D. Orobengoa, C. Capillas, J. M. Perez-Mato, and M. I. Aroyo. An introduction to the tools hosted

- in the Bilbao Crystallographic Server. *EPJ Web of Conferences*, 22:00009, 2012.
- [22] C. J. Bradley and Arthur P. Cracknell. *The mathematical theory of symmetry in solids: representation theory for point groups and space groups*. Oxford classic texts in the physical sciences. Clarendon Press, Oxford : New York, 2010.
- [23] G. F. Koster. Space Groups and Their Representations. In FREDERICK Seitz and DAVID Turnbull, editors, *Solid State Physics*, volume 5, pages 173–256. Academic Press, January 1957.
- [24] Martin T. Dove. *Structure and dynamics: an atomic view of materials*. Oxford master series in condensed matter physics. Oxford University Press, Oxford ; New York, 2003.
- [25] Wahyu Setyawan and Stefano Curtarolo. High-throughput electronic band structure calculations: Challenges and tools. *Computational Materials Science*, 49(2):299–312, August 2010.
- [26] Harald Ibach. *Physics of Surfaces and Interfaces*. Springer, Berlin; Heidelberg, 2006. OCLC: 780977739.
- [27] H. Ibach and H. Lüth. *Solid-state physics: an introduction to principles of materials science*. Advanced texts in physics. Springer, Berlin ; New York, 4th extensively updated and enlarged edition, 2009.
- [28] Armando Euceda, D. M. Bylander, and Leonard Kleinman. Self-consistent electronic structure of 6- and 18-layer Cu(111) films. *Physical Review B*, 28(2):528–534, July 1983.
- [29] C. Julian Chen. *Introduction to Scanning Tunneling Microscopy*. Oxford University Press, September 2007.
- [30] Samir Lounis. Theory of Scanning Tunneling Microscopy. *arXiv:1404.0961 [cond-mat]*, April 2014. arXiv: 1404.0961.
- [31] A. N. Chaika and A. N. Myagkov. Imaging atomic orbitals in STM experiments on a Si(111)-(77) surface. *Chemical Physics Letters*, 453(4):217–221, March 2008.
- [32] Dmitrij Rappoport, Nathan R M Crawford, Filipp Furche, and Kieron Burke. Which functional should I choose? page 25, December 2008.
- [33] Ohio Supercomputer Center. *Ohio Supercomputer Center*. 1987.
- [34] P Giannozzi, O Andreussi, T Brumme, O Bunau, M Buongiorno Nardelli, M Calandra, R Car, C Cavazzoni, D Ceresoli, M Cococcioni, N Colonna, I Carnimeo, A Dal Corso, S de Gironcoli, P Delugas, R A DiStasio, A Ferretti, A Floris, G Fratesi, G Fugallo, R Gebauer, U Gerstmann, F Giustino, T Gorni, J Jia, M Kawamura, H-Y Ko, A Kokalj, E Küçükbenli, M Lazzeri, M Marsili, N Marzari, F Mauri, N L Nguyen, H-V Nguyen, A Otero-de-la Roza, L Paulatto, S Poncé, D Rocca, R Sabatini, B Santra, M Schlipf, A P Seitsonen, A Smogunov, I Timrov, T Thonhauser, P Umari, N Vast, X Wu, and S Baroni. Advanced capabilities for materials modelling with Quantum ESPRESSO. *Journal of Physics: Condensed Matter*, 29(46):465901, November 2017.
- [35] Paolo Giannozzi, Stefano Baroni, Nicola Bonini, Matteo Calandra, Roberto Car, Carlo Cavazzoni, Davide Ceresoli, Guido L. Chiarotti, Matteo Cococcioni, Ismaila Dabo, Andrea Dal Corso, Stefano de Gironcoli, Stefano Fabris, Guido Fratesi, Ralph Gebauer, Uwe Gerstmann, Christos Gougoussis, Anton

- Kokalj, Michele Lazzeri, Layla Martin-Samos, Nicola Marzari, Francesco Mauri, Riccardo Mazzarello, Stefano Paolini, Alfredo Pasquarello, Lorenzo Paulatto, Carlo Sbraccia, Sandro Scandolo, Gabriele Scлаuzero, Ari P. Seitsonen, Alexander Smogunov, Paolo Umari, and Renata M. Wentzcovitch. QUANTUM ESPRESSO: a modular and open-source software project for quantum simulations of materials. *Journal of Physics: Condensed Matter*, 21(39):395502, 2009.
- [36] Andrea Dal Corso. Pseudopotentials periodic table: From H to Pu. *Computational Materials Science*, 95:337–350, December 2014.
- [37] I. Pletikosić, M. Kralj, D. Šokčević, R. Brako, P. Lazić, and P. Pervan. Photoemission and density functional theory study of Ir(111); energy band gap mapping. *Journal of Physics: Condensed Matter*, 22(13):135006, 2010.
- [38] I. Horcas, R. Fernández, J. M. Gómez-Rodríguez, J. Colchero, J. Gómez-Herrero, and A. M. Baro. WSXM: A software for scanning probe microscopy and a tool for nanotechnology. *Review of Scientific Instruments*, 78(1):013705, January 2007.
- [39] John W. Arblaster. Crystallographic Properties of Iridium. *Platinum Metals Review*, 54(2):93–102, April 2010.
- [40] Pin-Jui Hsu, Levente Rózsa, Aurore Finco, Lorenz Schmidt, Krisztián Palotás, Elena Vedmedenko, László Udvardi, László Szunyogh, André Kubetzka, Kirsten von Bergmann, and Roland Wiesendanger. Inducing skyrmions in ultrathin Fe films by hydrogen exposure. *Nature Communications*, 9(1):1571, April 2018.
- [41] Zhiyao Feng. *The Lattice Parameter of Gamma Iron and Iron-Chromium Alloys*. PhD thesis, Case Western Reserve University, 2015.
- [42] S. Heinze. Simulation of spin-polarized scanning tunneling microscopy images of nanoscale non-collinear magnetic structures. *Applied Physics A*, 85(4):407–414, December 2006.